iScience

CellPress

Article

Sensitivity to Oxygen in Microbial Electrochemical Systems Biofilms

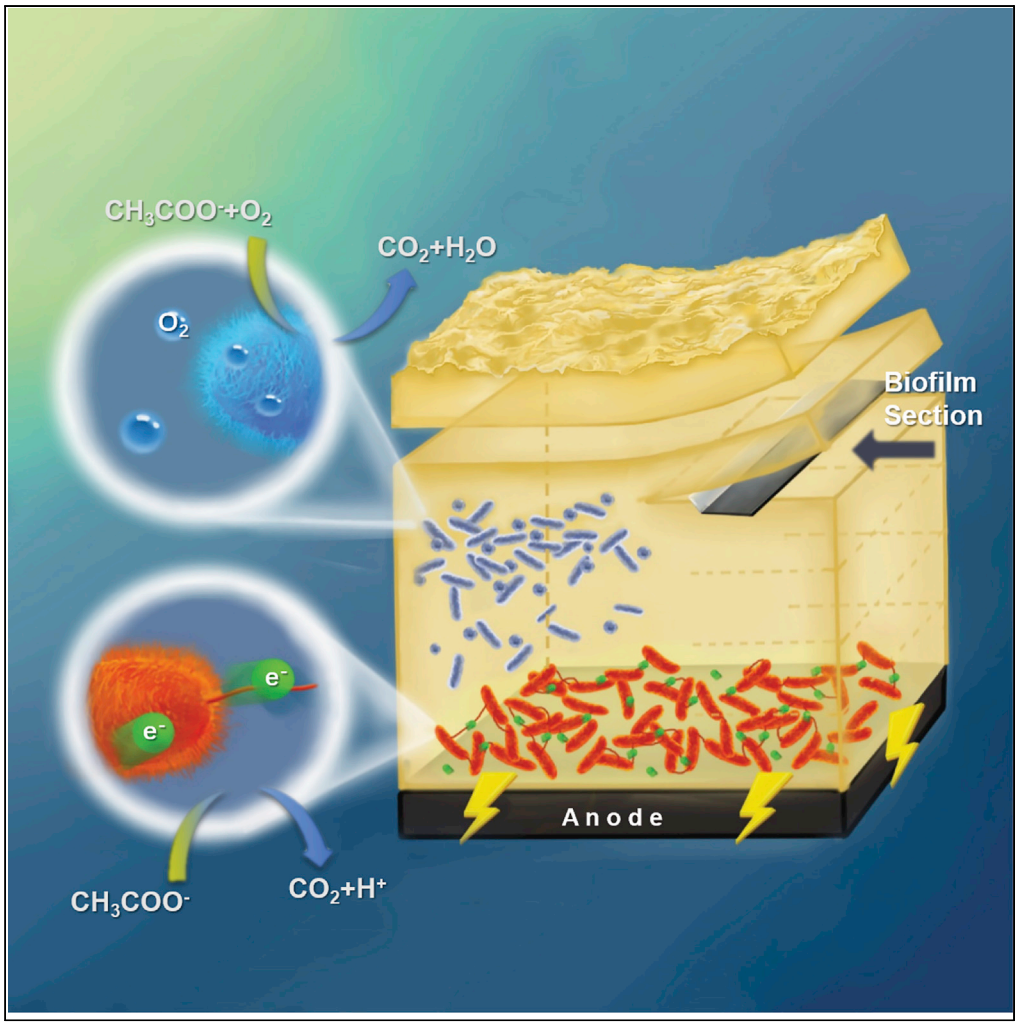

Jiawei Yang, Shaoan Cheng, Peng Li, Haobin Huang, Kefa Cen

shaoancheng@zju.edu.cn

HIGHLIGHTS

The growth of anode biofilm was observed *in situ* by optical coherence tomography

Anode biofilms were analyzed by frozen section coupled with gene sequencing

The aerobe-enriched anode biofilm showed a dual-layer structure

The outer layer consumed oxygen, and the inner layer performed electricity generation

Yang et al., iScience *13*, 163–172
March 29, 2019
https://doi.org/10.1016/j.isci.2019.01.022

iScience

CellPress

Article

Sensitivity to Oxygen in Microbial Electrochemical Systems Biofilms

Jiawei Yang,[1] Shaoan Cheng,[1,3,*] Peng Li,[2] Haobin Huang,[1] and Kefa Cen[1]

SUMMARY

The formation and bioelectric performance of anode biofilms in microbial electrochemical systems (MESs) are sensitive to oxygen. Investigating the temporal-spatial structure of anode biofilms will help elucidate the interfaces between oxygen and bacteria, thereby facilitating the applications of MESs in wastewater treatment and energy recovery. Here, use of optical coherence tomography, frozen sections, and a microsensor revealed that the aerobic biofilms exhibited a multilayered sandwich structure with a sparse gap between the aerobe- and amphimicrobe-enriched outer layer and the dense exoelectrogen-enriched inner layer, whereas the anaerobic biofilm consisted of only a single dense layer. Our results showed that the inner layer of aerobic anode biofilms performed electricity generation, whereas the outer layer only consumed oxygen. In this case, electron donor diffusion through the outer layer became the limiting factor in electricity generation by the bioanode. Consequently, as the anode biofilms matured, current generation decreased.

INTRODUCTION

Microbial electrochemical systems (MESs) represent promising technologies for wastewater treatment and energy recovery by using anode-respiring bacteria (ARB) as a biocatalyst to oxidize organic waste (Logan et al., 2008; Liu et al., 2005). Oxygen is a common and essential metabolic electron acceptor present in practical applications of MESs. The effect of oxygen on anode biofilms has drawn great attention because of its wide presence and selective toxicity to ARB. In the cultivation of pure-culture ARB, oxygen showed toxic effects on anaerobic ARB such as *Geobacter* (Caccavo et al., 1994; Lovley et al., 1993; Lin et al., 2004), but a positive effect on the growth and extracellular electron transfer (EET) of aerobic or facultative ARB such as *Shewanella* and *Pseudomonas* (Rabaey et al., 2005; TerAvest et al., 2014). In the cultivation of mixed-culture ARB, the effects of oxygen on the formation and current generation of mixed-culture anode were more complicated (Cheng et al., 2006; Oh et al., 2009; Fan et al., 2012; Quan et al., 2012, 2013). Directly pumping oxygen into an anode chamber led to approximately 100% voltage loss in a two-chambered microbial fuel cell (MFC) with cation exchange membrane as a separator (Oh et al., 2009). Due to the increasing oxygen crossover from the air cathode to the anode, decreasing the electrode spacing from 2 to 1 cm resulted in a considerable drop in the power density of the air cathode single-chamber MFC from 811 to 423 mW/m^2 (Cheng et al., 2006). However, some studies have reported a minor effect of oxygen on the anode biofilms, and the power density of a compact MFC with a J-cloth separator between the anode and cathode, which could start up in 5 days, decreased only from 1,700 to 1,400–1,600 W/m^3 when oxygen was directly pumped into the MFC chamber (Fan et al., 2012). Furthermore, Quan et al. reported that an anode biofilm could be formed under an air flow rate of 1.5 L/min and that the anaerobic-enriched biofilm showed a power generation loss of only 26% under aeration (Quan et al., 2012, 2013).

These discrepant results likely indicate that the anode biofilms formed under different conditions have different structures and oxygen sensitivities. Studying the spatiotemporal structure of anode biofilm during MFC start-up will facilitate a better understanding of the interfaces between oxygen and bacteria. To date, temporal-spatial structure investigations of anode biofilms have mainly involved confocal laser scanning microscopy (CLSM) and nuclear magnetic resonance (NMR) (Franks et al., 2009; Sun et al., 2015; Renslow et al., 2013a, 2013b). CLSM is an optical sectioning technique that acquires fluorescence signals within the sample. However, the toxicity of fluorochromes to microorganisms limits the utility of CLSM in temporal studies of anode biofilm formation. Moreover, the inadequate permeation of fluorochromes limits the utility of CLSM for dense or thick biofilm observations. Fortunately, NMR can be employed to circumvent this problem. Renslow et al. observed anode biofilm growth and analyzed electron transfer and substrate diffusion in biofilms by NMR. However, the physical properties of these films cannot be correlated with the microbial community by NMR, and the low resolution of NMR (>10 μm) is another disadvantage when

[1]State Key Laboratory of Clean Energy, Department of Energy Engineering, Zhejiang University, Hangzhou 310027, PR China

[2]State Key Lab of Modern Optical Instrumentation and the Collaborative Innovation Center for Brain Science, College of Optical Science and Engineering, Zhejiang University, Hangzhou, Zhejiang 310027, PR China

[3]Lead Contact

*Correspondence: shaoancheng@zju.edu.cn

https://doi.org/10.1016/j.isci.2019.01.022

examining anode biofilms (Renslow et al., 2013a, 2013b). Available analysis methods have a limited ability to correlate the anode biofilm structure to its performance. Therefore new methods for temporal-spatial studies of anode biofilms and their local structures must be developed.

Optical coherence tomography (OCT) is a new non-invasive, non-destructive, high-spatial-resolution, and real-time optical measurement technique for ophthalmologic imaging and material nondestructive testing (Huang et al., 1991; Xi et al., 2006). Compared with other morphological analysis technologies, such as scanning electron microscopy, CLSM, and magnetic resonance imaging (Franks et al., 2009; Renslow et al., 2013a, 2013b), OCT allows online morphological observations and does not damage the sample; therefore, it should be suitable for investigating anode biofilm formation online.

Tissue sections have been widely employed in pathology for structural analysis. These sections can be further analyzed by microscopy or extraction techniques to evaluate the spatial distribution of microbial communities, as successfully demonstrated using aerobic and anaerobic granular sludge samples (Lemaire et al., 2008). In 2010, Franks used sections in an MES for the first and, to our knowledge, only time (Franks et al., 2010). Specifically, microarray analysis of prepared sections successfully revealed that most genes had higher transcript abundances in the inner layer (0–20 μm from anode surface of the total 60-μm biofilm) of a *Geobacter sulfurreducens* biofilm. However, because a microtome was used to prepare the section, it had a thickness of only 100 nm and an area of 25 mm^2; thus it was only suitable for gene expression analysis. In this work, frozen anode biofilm sections with suitable size were prepared for genome analysis to investigate the structure of biofilms, especially mixed-culture biofilms.

In this study, the effects of oxygen on the formation and spatial structure of a mixed-culture anode biofilm were investigated with flowing nitrogen-oxygen mixtures (oxygen partial pressure of 0%–20%) over the anode surface. OCT was used to analyze anode biofilm formation in aerobic or anaerobic environments. Frozen sections coupled with high-throughput 16S rRNA sequencing were used to analyze the spatial community structure along the depth of the anode biofilm. The oxygen distribution along the depth of the biofilms was measured by a microelectrode. The electrochemical performance of the anode was evaluated by using linear sweep voltammetry (LSV) and electrochemical impedance spectroscopy (EIS).

RESULTS AND DISCUSSION

MFC Startup

All MFCs were successfully started under 0%–20% oxygen partial pressure (MFC configuration shown in Figure S1). The start-up process of all the MFCs went through three stages: the lag sage (referred to as stage A), in which the cell voltage varied by only a few millivolts; the rapid growth stage (referred to as stage B), in which the cell voltage rapidly increased to 360 mV in 1 day; and the stationary stage (referred to as stage C), in which the cell voltage maintained a constant value of 365 $\pm$ 5 mV, as shown in Figure 1. The lag time increased as the oxygen partial pressure increased from 0% to 20%, corresponding to an increase in the lag time of approximately 1 day per 5% increase in the oxygen partial pressure. A similar effect of oxygen on the lag stage of MFC start-up was reported by Quan et al. (Quan et al., 2013) and Choi et al. (Choi and Chae, 2013). In their studies, the lag stage extended from several hours to several tens of hours when oxygen was introduced. However, in stage B, the cell voltages of all MFCs rapidly increased to stable voltages in a short time. The oxygen concentration had little effect on the time of stage B for OPP-0, OPP-5, and OPP-10 and only slightly lengthened the time for OPP-15 and OPP-20. The stable voltages of the MFCs in stage C decreased from 365 $\pm$ 5 mV to 310 $\pm$ 5 mV as the oxygen partial pressure increased from 0% to 20%.

OCT Observations of Anode Biofilm Formation

During start-up, different formation processes were confirmed in the anode biofilms via *in situ* observations of anode biofilm formation using OCT. OCT images of the OPP-0 and OPP-20 anode biofilms collected at stages A (60 h for OPP-0 and 108 h for OPP-20), B (85 h for OPP-0 and 160 h for OPP-20), and C (180 h for OPP-0 and 250 h for OPP-20) are shown in Figure 2. For OPP-0, colonies were scattered across the electrode surface in stage A (Figure 2A), the colonies rapidly developed in the form of a hemisphere accumulated on the surface in stage B (Figure 2B), whereas at stage C, the colonies developed into a continuous biofilm with a thickness of 80 μm that covered the whole surface (Figure 2C). However, for OPP-20, a biofilm with a thickness of over 300 μm rapidly formed on the whole electrode surface in stage A (Figure 2D), whereas at stage B, the anode biofilm developed into a stratified structure with a thick outer layer (300–400 μm) and

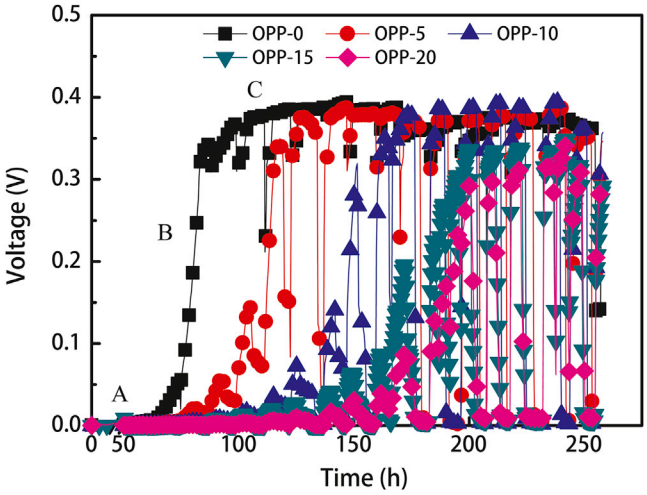

Figure 1. Electricity Generation of the Anode Biofilms at Different Oxygen Partial Pressures during Startup
A, the lag stage; B, the rapid growth stage; and C, the stationary stage.

a thin inner layer (20 μm) separated by a gap (Figure 2E). At stage C, the outer layer maintained a constant thickness of 300–400 μm, whereas the inner layer increased to 30–50 μm in thickness. In addition, a thorn-like structure formed on the outer layer along the direction of the air flow (white arrow) (Figure 2F), which was probably due to biofilm detachment. When a small fragment was sloughed off the biofilm, the rest of the biofilm was lifted by the air flow to form a surface cluster.

Spatial Microbial Community Structures of Anode Biofilms

Figure 3 shows the distribution of the predominant bacterial genera (details shown in Figure S3) along the anode biofilm thickness. The OPP-0 anode biofilm community mainly consisted of anaerobic *Geobacter* species (GenBank: FW306010.1) (Figure 3A). The relative abundances of the *Geobacter* species decreased along the biofilm thickness direction from the interior (electrode surface side, 80%) to the surface (solution side, 22%), whereas the relative abundances of the other predominant bacterial species gradually increased along the biofilm thickness direction from the interior to the surface. For example, the relative abundances of the *Azoarcus* (GenBank: AF011343.1), *Dechloromonas* (GenBank: AY945919.1), *Aminiphilus* (GenBank: GQ181552.1), and *Arcobacter* (GenBank: FJ968634.1, GenBank: FJ968635.1) species increased from 2% to 14%, from 3% to 10%, from 3% to 7%, and from 1% to 8%, respectively. Among them, *Azoarcus* species are facultative anaerobic bacteria owing to their nitrogen fixation abilities (Reinhold-hurek et al., 1993), both *Dechloromonas* (Wolterink et al., 2005) and *Aminiphilus* (Diaz et al., 2007) are anaerobic bacteria, and *Arcobacter* (Fedorovich et al., 2009) are facultative aerobic bacteria (microaerobic, favoring growth under an oxygen partial pressure of 3%–10%). Thus the OPP-0 biofilm consisted of only one layer of predominantly anaerobic and facultative anaerobic bacteria, which is consistent with the OCT observation.

When oxygen was introduced into the system, no new species of electrochemical active bacteria were found in all the anode biofilms, and significant changes were not observed in other dominant bacterial species or their relative abundances in the interior biofilm, but significant changes were observed in the dominant bacterial species and their relative abundances along the thickness direction from the interior to the surface. In the interior biofilm, the dominant bacterial species and their relative abundances were similar. For example, the relative abundances of the dominant bacterial species *Geobacter, Dechloromonas, Desulfovibrio,* and *Aminiphilus* in the electrode surface of OPP-0 (80%, 2.7%, 1.7%, and 3%) and OPP-5 (77%, 1.3%, 1.6%, and 3.3%) were quite similar. However, along the thickness direction from the interior to the surface, for the OPP-5 anode biofilm, the relative abundances of *Geobacter* species (GenBank: FW306010.1) decreased from 77% (5 μm) to 56% (50 μm) and then to 1.5% ± 1% (>100 μm) (Figure 3B) along the thickness direction of the biofilm, whereas the relative abundances of the *Arcobacter* (GenBank: FJ968634.1, GenBank: FJ968635.1), *Acinetobacter* (GenBank: HQ670708.1), *Pseudomonas* (GenBank: HM451438.1), and *Azoarcus* (GenBank: AF011343.1) species were 1% at a biofilm thickness of 5 μm and

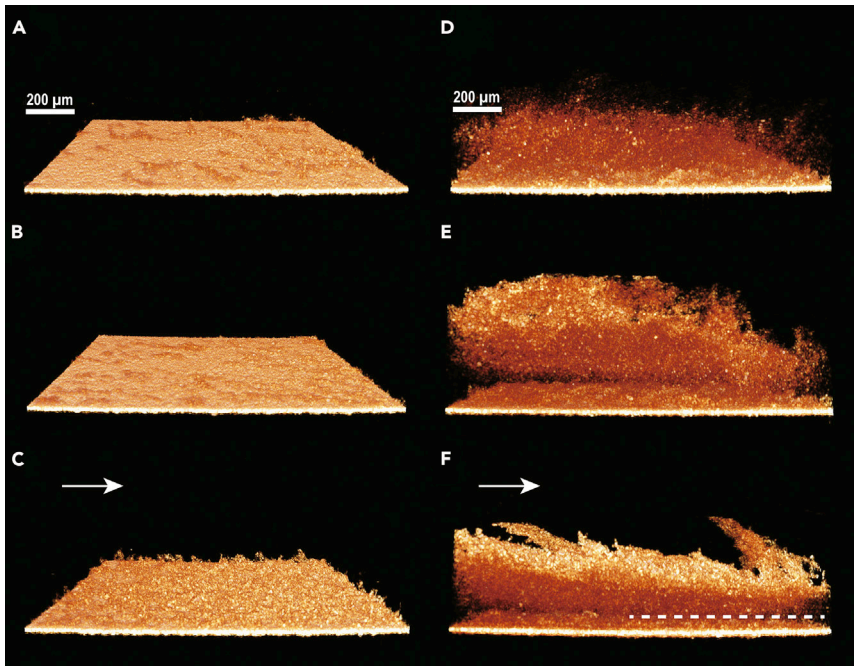

Figure 2. 3D OCT Images Showing Anode Biofilm Formation during Startup

(A–F) (A) Lag, (B) rapid growth, and (C) stationary stages for the OPP-0 biofilm; (D) lag, (E) rapid growth, and (F) stationary stages for the OPP-20 biofilm. The dashed line in (F) indicates the sparse gap between the dense inner layer and the dense outer layer. The white arrows in (C) and (F) indicate the gas flow direction. The scale bar represents 200 μm.

increased to 3.5%, 13%, 2%, and 3% at a thickness of 50 μm, respectively, and then to 29% ± 2%, 29% ± 1%, 7% ± 2%, and 11% ± 2% at a thickness of over 100 μm, respectively. Among them, *Azoarcus* and *Arcobacter* (which favor growth under an oxygen partial pressure of 3%–10%) are facultative bacteria, and *Acinetobacter* (Juni, 1972) and *Pseudomonas* (Palleroni, 2010) are generally strictly aerobic bacteria. When the oxygen partial pressure was increased to 15%, the relative abundances of the *Geobacter* species in the biofilm decreased from 67% to 0% along the thickness direction from 0 to 50 μm and then remained at 0 over 50 μm (Figure 3C), whereas the relative abundances of the *Pseudomonas* species rapidly increased from 13% to 60% along the thickness direction from 0 to 50 μm and then remained at 60% ± 10% over 50 μm. For other predominant bacterial species in the OPP-15 biofilm, the relative abundances along the thickness direction from 0 to 100 μm of the strictly aerobic bacteria *Comamonas* (Tago and Yokota, 2004) increased from 1% to 6% ± 2% and of the *Arcobacter* and *Acinetobacter* species increased from 0% to 3% ± 1% and from 3% to 9% ± 2%, respectively. Both OPP-5 and OPP-15 had similar relative abundances of *Azoarcus* species (10%–15%) in the outer layer of the biofilm along the thickness direction over 100 μm. Thus the anode biofilm that formed under aerobic conditions presented a dual-layer structure. The anaerobic *Geobacter* species dominated the inner layer, whereas aerobic genera such as *Acinetobacter*, *Pseudomonas*, and *Comamonas* and facultative genera such as *Arcobacter* dominated the outer layer. The dual-layer structure was consistent with the OCT observations.

Oxygen Distributions in Anode Biofilms

The dissolved oxygen (DO) distributions in the anode biofilms are shown in Figure 4 (replication shown in Figure S4). For OPP-0, the DO concentration was less than 0.3 mg/L throughout the entire biofilm, which is consistent with the results of previous studies (Chang et al., 2014; Zhang et al., 2013). For the reactors bubbled with oxygen, the DO concentration in the solution corresponds to the saturation oxygen concentration under each oxygen partial pressure, with 1.7 mg/L for OPP-5 and 5.4 mg/L for OPP-15, whereas the DO concentration in the biofilm presented a gradient distribution along the thickness direction. For OPP-5, the DO concentration maintained a constant value of 1.7 mg/L in the solution phase, gradually decreased from 1.7 mg/L at the biofilm surface (360 μm from the electrode surface) to 0 mg/L at a distance of 200 μm from the electrode surface, and then was maintained at 0 mg/L at distances from 200 to 0 μm away from the electrode surface. When the bubbled oxygen partial pressure increased to 15% (OPP-15), the saturated DO

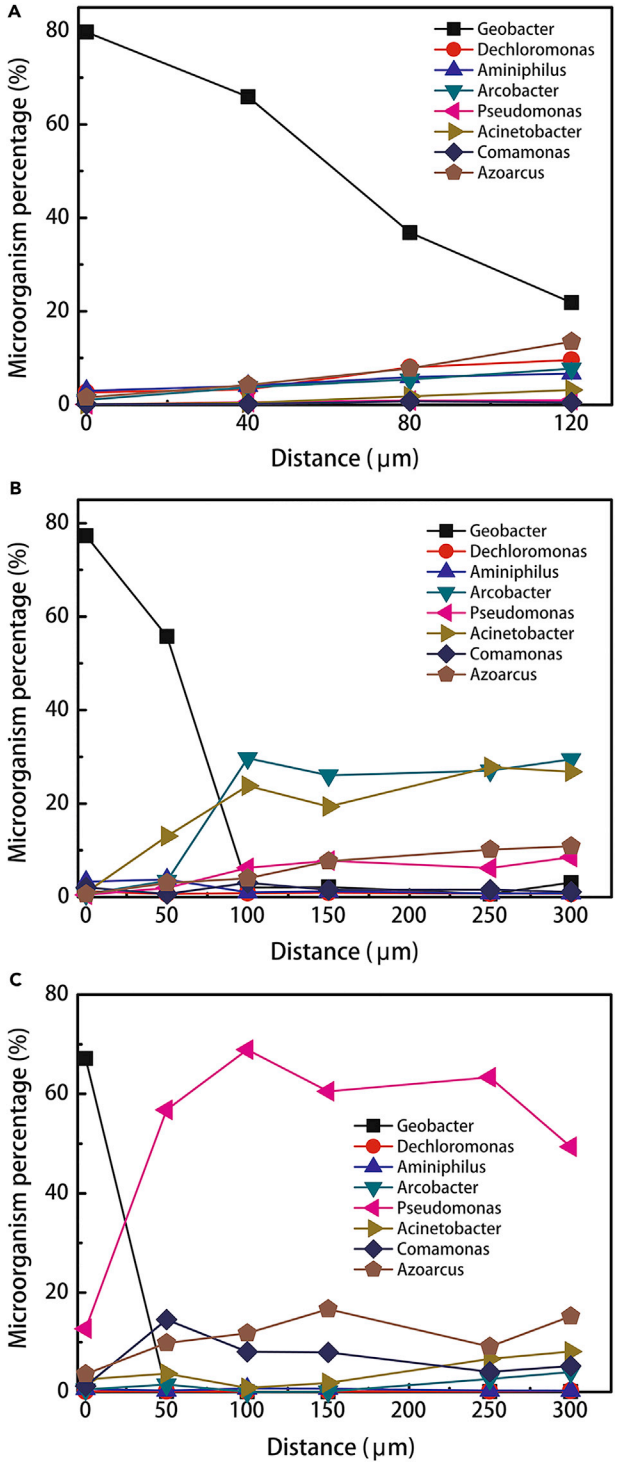

Figure 3. Spatial Distributions of the Anode Biofilm Microbial Communities

(A) OPP-0, (B) OPP-5, and (C) OPP-15 samples. See also Figure S3. A distance of 0 μm corresponds to the graphite plate surface and the last obtained frozen section.

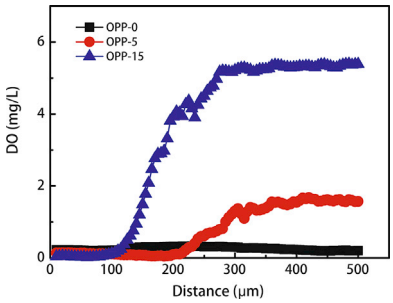

Figure 4. Oxygen Distributions in the OPP-0, OPP-5, and OPP-15 Anode Biofilms

The distance 0 μm represents the graphite anode surface. See also Figure S4.

concentration in the solution phase increased to 5.4 mg/L, whereas the DO concentration in the biofilm gradually decreased from 5.4 mg/L at the biofilm surface (260 μm from the electrode surface) to 0 mg/L at a distance of 100 μm and was then maintained at 0 mg/L at distances from 100 to 0 μm away from the electrode surface. The thickness of the biofilm in the anaerobic environment (0 mg/L DO) decreased as the bubbling oxygen concentration increased.

Formation and Function of Dual-Layer Anode Biofilms

During start-up, oxygen greatly extended the lag stage but had a minor effect on the rapid growth stage (Figure 1). The variation in MFCs' start-up was attributed to the effects of oxygen on anode performance rather than cathode performance as the oxygen permeated from anode to cathode was found to have a minor influence on the cathode performance. The cathode potentials of all the MFCs were measured at the three stages (the lag stage, the rapid growth stage, and the stationary stage) of start-up process. The variations of cathode potential were less than 0.005 V for all the MFCs after the anode chamber was aerated with a gas mixture of each oxygen partial pressure. The OCT observations of OPP-20 showed that a 300-μm-thick biofilm formed on the electrode surface in the lag stage when the cell voltage was only a few millivolts (Figure 2D). Interestingly, the anode structure became stratified as the electricity generation rapidly increased. These results most likely indicate that the inner layer performed electricity generation, whereas the outer layer provided a suitable environment for exoelectrogen growth on the electrode surface or electron transfer from the exoelectrogens to the electrode. The difference in the terminal electron acceptor of the outer and inner layers probably resulted in the formation of loose gap between the outer and inner layers. It was previously shown that a *Geobacter* biofilm had a higher density near the electrode surface when the terminal electron acceptor was the anode (Jain et al., 2011; Renslow et al., 2013b). In contrast, biofilms in which oxygen acts as the terminal electron acceptor have higher densities at the biofilm-solution interface (far from the electrode surface).

Further investigation of the spatial microbial community structures showed that the inner layer was dominated by the anaerobic *Geobacter* species, whereas the outer layer was dominated by aerobic genera such as *Acinetobacter*, *Pseudomonas,* and *Comamonas* and facultative genera such as *Arcobacter*. *Geobacter* species (FW306010.1) present in the inner layer have been reported to have strong electricity generation ability (Bond and Lovley, 2003). The *Arcobacter* species (FJ968634.1, FJ968635.1) present in the outer layer were also reported to be electrochemically active (Fedorovich et al., 2009), whereas the *Acinetobacter* (HQ670708.1), *Pseudomonas* (HM451438.1), and *Comamonas* (AB021357.1) species were not reported to be electrochemically active. In an aerobic environment, *Arcobacter*, *Acinetobacter*, *Pseudomonas,* and *Comamonas* are more likely to transfer electron to oxygen rather than to electrode, without electricity generation. Thus the spatial microbial community structures also suggested that the inner layer performed electricity generation, whereas the outer layer consumed oxygen. In this case, an anaerobic environment is most likely necessary for the growth and electricity generation of exoelectrogens. The increasing lag stage with the oxygen partial pressure in the bubbled gas was due to the increased time required to grow the thick aerobic biofilm, which is necessary for the development of an anaerobic environment on the electrode surface.

To further confirm that only the anaerobic bacteria in the inner-layer biofilm were responsible for electricity generation, gentamicin and metronidazole were selected to inhibit the activity of outer- and inner-layer bacteria, respectively. Metronidazole is known for its bactericidal activity, mainly against anaerobic bacteria and methanogenic archaea (Martin et al., 1972; Löfmark et al., 2010; Dione et al., 2015). However,

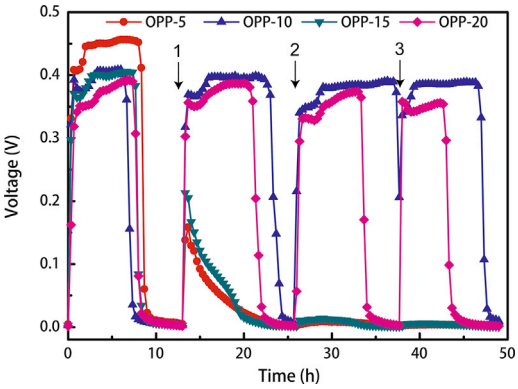

Figure 5. Cell Voltage Evolution over Batch Cycles for Reactors with and without the Addition of Antibiotics

For OPP-5 and OPP-15, 120 mg/L metronidazole was added in cycles **1** and **3**. For OPP-10 and OPP-20, 48 mg/L gentamicin was added in cycles **1** and **3**. All antibiotics were removed in cycle **2**.

metronidazole has minimal effects against aerobic and facultative aerobic bacteria (Martin et al., 1972; Dione et al., 2015). Gentamicin, in contrast, displays bactericidal activity against gram-negative aerobes, but generally not against anaerobic bacteria (Pacific and Marchini, 2017). The effective antibiotic activity of gentamicin against *Acinetobacter* (Anstey et al., 1992), *Pseudomonas* (Dione et al., 2015), and *Arcobacter* (Córdoba-Calderón et al., 2017) has been verified. As shown in Figure 5, after metronidazole was added to the OPP-5 and OPP-15 MFCs, electricity generation ceased in 10 h and the cell voltage could not be recovered when the anode solution was refreshed. In contrast, when gentamicin was added to OPP-10 and OPP-20, the cell voltages of the MFCs only decreased by less than 10 mV in one cycle and the cycle time increased from 7 h to 12 h. These results further suggest that only the anaerobic bacteria in the inner layer were responsible for electricity generation.

Electrochemical Properties of Anode Biofilms

The electrochemical properties of the anode biofilm were evaluated by using the LSV. Figure 6A shows the LSV results with 1.5 g/L acetate; all the anode biofilms showed a significant increase in the current density at −0.48 V (versus Ag/AgCl) and reached a peak current at −0.35 V. For the anode biofilm enriched in the anaerobic environment (OPP-0), the peak current density was 2.44 A/m^2, whereas for the anodes enriched in aerobic environments, the peak current densities decreased significantly. The peak current densities of OPP-5, OPP-10, OPP-15, and OPP-20 were 1.34 A/m^2, 0.89 A/m^2, 0.55 A/m^2, and 0.32 A/m^2, respectively. A linear relationship was observed between the natural logarithm of the peak current density and the oxygen partial pressure.

The Nyquist plots (Figure 6B) obtained from the EIS test of anode in MFCs was usually fitted using a two-time-constant model, $R_s(R_{ct}Q_1)(R_dQ_2)$, for resistance estimation (Hou et al., 2014; Yang et al., 2017). In this model, R_s represents the anode resistance, R_{ct} represents the charge transfer resistance, R_d represents the diffusion resistance, and Q_1 and Q_2 are the constant phase angle elements. As shown in Figure 6B, the solution resistance R_s of all the MFCs was approximately 19.5 Ω. In contrast, the charge transfer resistance R_{ct} and the diffusion resistance R_d increased with increasing oxygen partial pressure used during anode start-up, and both showed a linear relationship between the natural logarithm value and the oxygen partial pressure. Compared with OPP-0, OPP-20 had R_{ct} values that were 3.5 times higher (252 Ω versus 55.9 Ω) and R_d values that were 249 times higher (50 Ω versus 0.2 Ω).

The EIS results indicated that the decreased electricity generation of the MFCs with aerobic anode biofilms was mainly due to their higher diffusion and charge transfer resistances. Increasing oxygen had a much greater effect on R_d than on R_{ct}, indicating that higher diffusion resistance is the key factor affecting anode performance. The natural logarithm of R_d exhibited a linear relationship with the oxygen partial pressure, indicating that the diffusion of electron donors to or protons from the biofilm was strongly affected. This limited diffusion will strongly inhibit the growth and electrogenesis of the inner layer and cause cell death and biofilm detachment (Renslow et al., 2013a; Sun et al., 2015), thereby leading to a decrease in the inner-layer thickness. The limited growth of exoelectrogens will result in an increase in charge transfer resistance. Regardless of the specific form of EET, which can be either conduction- or diffusion-based (mediated) mechanisms or a combination of mechanisms, the limited growth of exoelectrogens will lead to increased electrical resistance by reducing either the quantity of electron shuttles or the quantity of components that exhibit metal-like conduction (Strycharz-Glaven et al., 2011).

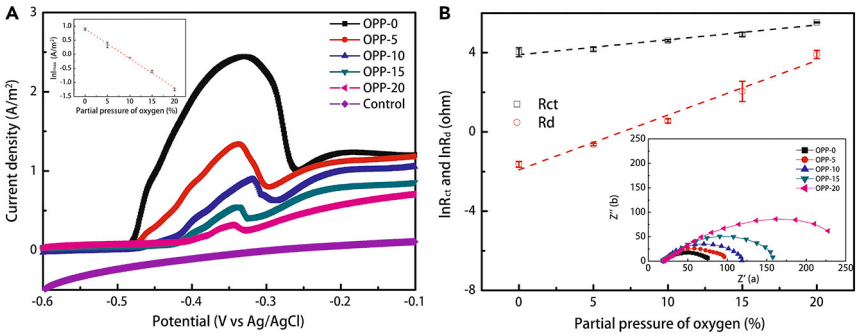

Figure 6. Electrochemical Properties of the Anode Biofilms Formed at Different Oxygen Partial Pressures

(A) Currents generated by the anode biofilms formed at different oxygen partial pressures in 50 mM PBS containing 1.5 g/L acetate.

(B) Linear relationships between the natural logarithms of the charge transfer resistance ($\ln(R_{ct})$) and diffusion resistance ($\ln(R_d)$) and the oxygen partial pressure. Control was a polished graphite plate anode without biofilm. The inset in (A) shows the linear relationship between the natural logarithm of the peak current density ($\ln(I_{max})$) and the oxygen partial pressure. The inset in (B) shows the Nyquist plots of the EIS spectra and the equivalent circuit. The error bars represent standard error of duplicate replicates.

In this study, we revealed for the first time that an anaerobically enriched anode biofilm consisted of a single-layer structure and an aerobically enriched anode biofilm consisted of a dual-layer structure with the inner layer dominated by anaerobic bacteria and the outer layer dominated by aerobic bacteria. These results were confirmed by *in situ* OCT observations together with high-throughput 16S rRNA sequencing coupled with frozen sections. It was found that the function of the inner layer of aerobically formed anode biofilm was electricity generation, whereas the function of the outer layer was as a barrier for oxygen to realize anaerobic environment for the inner layer. However, thick outer layer will hinder the diffusion of substrate and proton in the biofilm, resulting in the reduction of electricity generation. These results implied that high power density in aerobic condition could be only generated with an oxygen-tolerant anode biofilm with thin outer layer and thick inner layer. This is significantly importance for developing the compacted electrode assembly air cathode MFCs, which had been considered as ideal configuration for high power generation (Fan et al., 2012). Future works should focus on developing methods to regulate and control the formation of anode biofilm with this structure.

In addition, the combined technology is useful for investigation of bioanodes. OCT provided a useful tool for performing *in situ* observations of the formation process of an anode biofilm and identifying the relationship between biofilm structure and electricity generation. Further studies of biofilm formation and structural changes during the long-term operation of MFCs under different conditions by using OCT coupled with frozen section sequencing will help clarify why an anode biofilm could maintain a constant thickness during long-term operations. This information will facilitate the development of highly aerotolerant anodes for high-performance MFC and multifunctional biofilms for efficiently removing the chemical oxygen demand and other pollutants in wastewaters.

Limitations of the Study

Here, we showed how the presence of oxygen influences biofilm formation on a microbial anode and the consequences in electricity production. Performance of the cell is affected by choices such as high DO and distance of electrodes, which were not explored in the present study. We obtained the results with duplicate tests, which in general were not sufficient to have reproducible results. The two-layer structure of the aerobic anode biofilms provides a model for developing aerotolerant anodes. However, the performance of these anodes should be further improved, possibly by increasing substrate diffusion through them. Further efforts would be focused on the construction of high-performance aerotolerant anodes to facilitate the applications of MESs in wastewater treatment and energy recovery.

METHODS

All methods can be found in the accompanying Transparent Methods supplemental file.

SUPPLEMENTAL INFORMATION

Supplemental Information includes Transparent Methods and four figures and can be found with this article online at https://doi.org/10.1016/j.isci.2019.01.022.

ACKNOWLEDGMENTS

This work was supported by the National Natural Science Foundation of China (No. 51478414, No. 51778562) and the National Key Research and Development Plan (2016YFB0600505). We thank Jianyu Ni for providing the multimeter and stepper motor.

AUTHOR CONTRIBUTIONS

J.Y. and S.C. designed research, analyzed and interpreted majority of experimental data, and wrote the manuscript. P.L. performed and analyzed the optical imaging. H.H. analyzed microbial community. S.C. and K.C. assembled and directed the team, guided the project, and provided laboratory space.

DECLARATION OF INTERESTS

The authors declare no competing interests.

Received: October 4, 2018
Revised: December 23, 2018
Accepted: January 15, 2019
Published: March 29, 2019

REFERENCES

Anstey, N.M., Currie, B.J., and Withnall, K.M. (1992). Community-acquired *Acinetobacter pneumonia* in the northern territory of Australia. Clin. Infect. Dis. *14*, 83–91.

Bond, D.R., and Lovley, D.R. (2003). Electricity production by *Geobacter sulfurreducens* attached to electrodes. Appl. Environ. Microbiol. *69*, 1548–1555.

Caccavo, F., Lonergan, D., Lovley, D.R., Davis, M., Stolz, J.F., and Mcinerney, M.J. (1994). *Geobacter sulfurreducens* sp. Nov., A hydrogen- and acetate oxidizing dissimilatory metal-reducing microorganism. Appl. Environ. Microbiol. *60*, 3752–3759.

Chang, S., Wu, C., Chang, D., and Lin, C. (2014). Effects of mediator producer and dissolved oxygen on electricity generation in a baffled stacking microbial fuel cell treating high strength molasses wastewater. Int. J. Hydrogen Energy *39*, 11722–11730.

Cheng, S., Liu, H., and Logan, B.E. (2006). Increased power generation in a continuous flow MFC with advective flow through the porous anode and reduced electrode spacing. Environ. Sci. Technol. *40*, 2426–2432.

Choi, S., and Chae, J. (2013). Optimal biofilm formation and power generation in a micro-sized microbial fuel cell (MFC). Sensor. Actuator Phys. *195*, 206–212.

Córdoba-Calderón, O., Redondo-Solano, M., Castro-Arias, E., and Arias-Echandl, M.L. (2017). *Arcobacter* isolation from minced beef samples in Costa Rica. J. Food Protect. *80*, 775–778.

Diaz, C., Baena, S., Fardeau, M.L., and Patel, B.K.C. (2007). *Aminiphilus circumscriptus* gen. Nov., Sp. Nov., an anaerobic amino-acid-degrading bacterium from an upflow anaerobic sludge reactor. Int. J. Syst. Evol. Microbiol. *57*, 1914–1918.

Dione, N., Khelaifia, S., Lagier, J., and Raoult, D. (2015). The aerobic activity of metronidazole against anaerobic bacteria. Int. J. Antimicrob. Agents *45*, 537–540.

Fan, Y., Han, S., and Liu, H. (2012). Improved performance of CEA microbial fuel cells with increased reactor size. Energ. Environ. Sci. *5*, 8273–8280.

Fedorovich, V., Knighton, M.C., Pagaling, E., Ward, F.B., Free, A., and Goryanin, I. (2009). Novel electrochemically active bacterium phylogenetically related to *Arcobacter butzleri*, isolated from a microbial fuel cell. Appl. Environ. Microbiol. *75*, 7326–7334.

Franks, A.E., Nevin, K.P., Glaven, R.H., and Lovley, D.R. (2010). Microtoming coupled to microarray analysis to evaluate the spatial metabolic status of *Geobacter sulfurreducens* biofilms. ISME J. *4*, 509–519.

Franks, A.E., Nevin, K.P., Jia, H., Izallalen, M., Woodard, T.L., and Lovley, D.R. (2009). Novel strategy for three-dimensional real-time imaging of microbial fuel cell communities: Monitoring the inhibitory effects of proton accumulation within the anode biofilm. Energ. Environ. Sci. *2*, 113–119.

Hou, J., Liu, Z., Yang, S., and Zhou, Y. (2014). Three-dimensional macroporous anodes based on stainless steel fiber felt for high-performance microbial fuel cells. J. Power Sources *258*, 204–209.

Huang, D., Swanson, E.A., Lin, C.P., Schuman, J.S., Stinson, W.G., Chang, W., Hee, M.R., Flotte, T., Gregory, K., Puliafito, C.A., et al. (1991). Optical coherence tomography. Science *254*, 1178–1181.

Jain, A., Gazzola, G., Panzera, A., Zanoni, M., and Marsili, E. (2011). Visible spectroelectrochemical characterization of *Geobacter sulfurreducens* biofilms on optically transparent indium tin oxide electrode. Electrochim. Acta *56*, 10776–10785.

Juni, E. (1972). Interspecies transformation of acinetobacter: genetic evidence for a ubiquitous genus. J. Bacteriol. *112*, 917–931.

Lemaire, R., Yuan, Z., Blackall, L.L., and Crocetti, G.R. (2008). Microbial distribution of *Accumulibacter* spp. and *Competibacter* spp. in aerobic granules from a lab-scale biological nutrient removal system. Environ. Microbiol. *10*, 354–363.

Lin, W.C., Coppi, M.V., and Lovley, D.R. (2004). *Geobacter sulfurreducens* can grow with oxygen as a terminal electron acceptor. Appl. Environ. Microbiol. *70*, 2525–2528.

Liu, H., Cheng, S., and Logan, B.E. (2005). Production of electricity from acetate or butyrate using a single-chamber microbial fuel cell. Environ. Sci. Technol. *39*, 658–662.

Löfmark, S., Edlund, C., and Nord, C.E. (2010). Metronidazole is still the drug of choice for treatment of anaerobic infections. Clin. Infect. Dis. *50*, S16–S23.

Logan, B.E., Call, D., Cheng, S., Hamelers, H.V.M., Sleutels, T.H.J.A., Jeremiasse, A.W., and Rozendal, R.A. (2008). Microbial electrolysis cells for high yield hydrogen gas production from organic matter. Environ. Sci. Technol. *42*, 8630–8640.

Lovley, D.R., Giovannoni, S.J., White, D.C., Champine, J.E., Phillips, E.J., Gorby, Y.A., and

Goodwin, S. (1993). *Geobacter metallireducens* gen. Nov. Sp. Nov., a microorganism capable of coupling the complete oxidation of organic compounds to the reduction of iron and other metals. Arch. Microbiol. *159*, 336–344.

Martin, W.J., Gardner, M., and Washington, J.A., II (1972). In vitro antimicrobial susceptibility of anaerobic bacteria isolated from clinical specimens1. Antimicrob. Agents Chemother. *1*, 148–158.

Oh, S.E., Kim, J.R., Joo, J.H., and Logan, B.E. (2009). Effects of applied voltages and dissolved oxygen on sustained power generation by microbial fuel cells. Water Sci. Technol. *60*, 1311–1317.

Pacific, G.M., and Marchini, G. (2017). Clinical pharmacokinetics of gentamicin in neonates. Int. J. Pediatr. *5*, 4575–4599.

Palleroni, N.J. (2010). The *Pseudomonas* story. Environ. Microbiol. *12*, 1377–1383.

Quan, X., Quan, Y., and Tao, K. (2012). Effect of anode aeration on the performance and microbial community of an air–cathode microbial fuel cell. Chem. Eng. J. *210*, 150–156.

Quan, X., Quan, Y., Tao, K., and Jiang, X. (2013). Effect of anode aeration on the performance and microbial community of an air-cathode microbial fuel cell. Bioresource Technol. *128*, 259–265.

Rabaey, K., Boon, N., Hofte, M., and Verstraete, W. (2005). Microbial phenazine production enhances electron transfer in biofuel cells. Environ. Sci. Technol. *39*, 3401–3408.

Reinhold-hurek, B., Hurek, T., Gillis, M., Hoste, B., Vancanneyt, M., Kersters, K., and Deley, J. (1993). *Azoarcus* gen, nov., nitrogen-fixing proteobacteria associated with roots of Kallar grass (*Leptochloa fusca* (L.) Kunth), and description of two species, *Azoarcus indigens* sp. Nov. and *Azoarcus communis* sp. Nov. Int. J. Syst. Bacteriol. *43*, 574–584.

Renslow, R.S., Babauta, J.T., Dohnalkova, A.C., Boyanov, M.I., Kemner, K.M., Majors, P.D., Fredrickson, J.K., and Beyenal, H. (2013a). Metabolic spatial variability in electrode-respiring *Geobacter sulfurreducens* biofilms. Energ. Environ. Sci. *6*, 1827–1836.

Renslow, R.S., Babauta, J.T., Majors, P.D., and Beyenal, H. (2013b). Diffusion in biofilms respiring on electrodes. Energ. Environ. Sci. *6*, 595–607.

Strycharz-Glaven, S.M., Snider, R.M., Guiseppi-Elie, A., and Tender, L.M. (2011). On the electrical conductivity of microbial nanowires and biofilms. Energ. Environ. Sci. *4*, 4366–4379.

Sun, D., Cheng, S., Wang, A., Li, F., Logan, B.E., and Cen, K. (2015). Temporal-spatial changes in viabilities and electrochemical properties of anode biofilms. Environ. Sci. Technol. *49*, 5227–5235.

Tago, Y., and Yokota, A. (2004). *Comamonas badia* sp. Nov., A floc-forming bacterium isolated from activated sludge. J. Gen. Appl. Microbiol. *50*, 243–248.

TerAvest, M.A., Rosenbaum, M.A., Kotloski, N.J., Gralnick, J.A., and Angenent, L.T. (2014). Oxygen allows *Shewanella oneidensis* MR-1 to overcome mediator washout in a continuously fed bioelectrochemical system. Biotechnol. Bioeng. *111*, 692–699.

Wolterink, A., Kim, S., Muusse, M., Kim, I.S., Roholl, P.J.M., van Ginkel, C.G., Stams, A.J.M., and Kengen, S.W.M. (2005). *Dechloromonas hortensis* sp. Nov. And strain ASK-1, two novel (per) chlorate-reducing bacteria, and taxonomic description of strain GR-1. Int. J. Syst. Evol. Microbiol. *55*, 2063–2068.

Xi, C., Marks, D., Schlachter, S., Luo, W., and Boppart, S.A. (2006). High-resolution three-dimensional imaging of biofilm development using optical coherence tomography. J. Biomed. Opt. *11*, 34001.

Yang, J., Cheng, S., Sun, Y., and Li, C. (2017). Improving the power generation of microbial fuel cells by modifying the anode with single-wall carbon nanohorns. Biotechnol. Lett. *39*, 1515–1520.

Zhang, X., Shi, J., Liang, P., Wei, J., Huang, X., Zhang, C., and Logan, B.E. (2013). Power generation by packed-bed air-cathode microbial fuel cells. Bioresource Technol. *142*, 109–114.

ISCI, Volume *13*

Supplemental Information

Sensitivity to Oxygen in Microbial Electrochemical Systems Biofilms

Jiawei Yang, Shaoan Cheng, Peng Li, Haobin Huang, and Kefa Cen

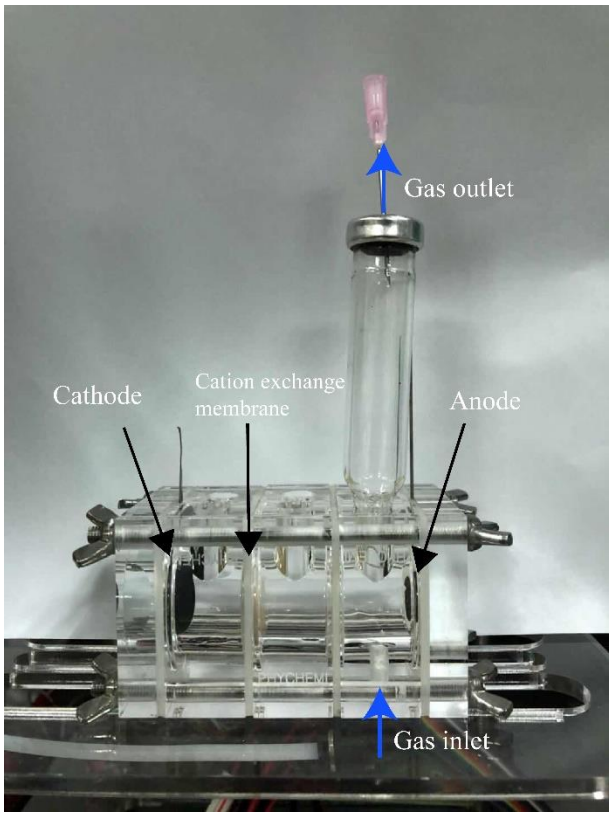

Figure S1. Photograph of MFC. Related to Figure 1, Figure 5, Figure 6 and Transparent Methods.

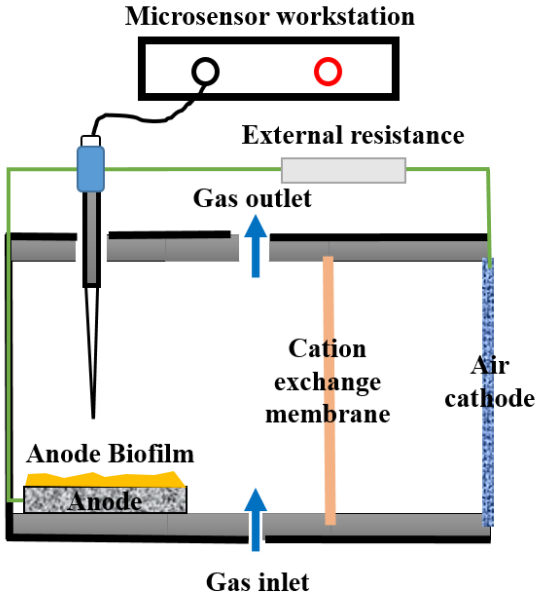

Figure S2. Schematic of the oxygen measurement experiment set-up. Related to Figure 4 and Transparent Methods.

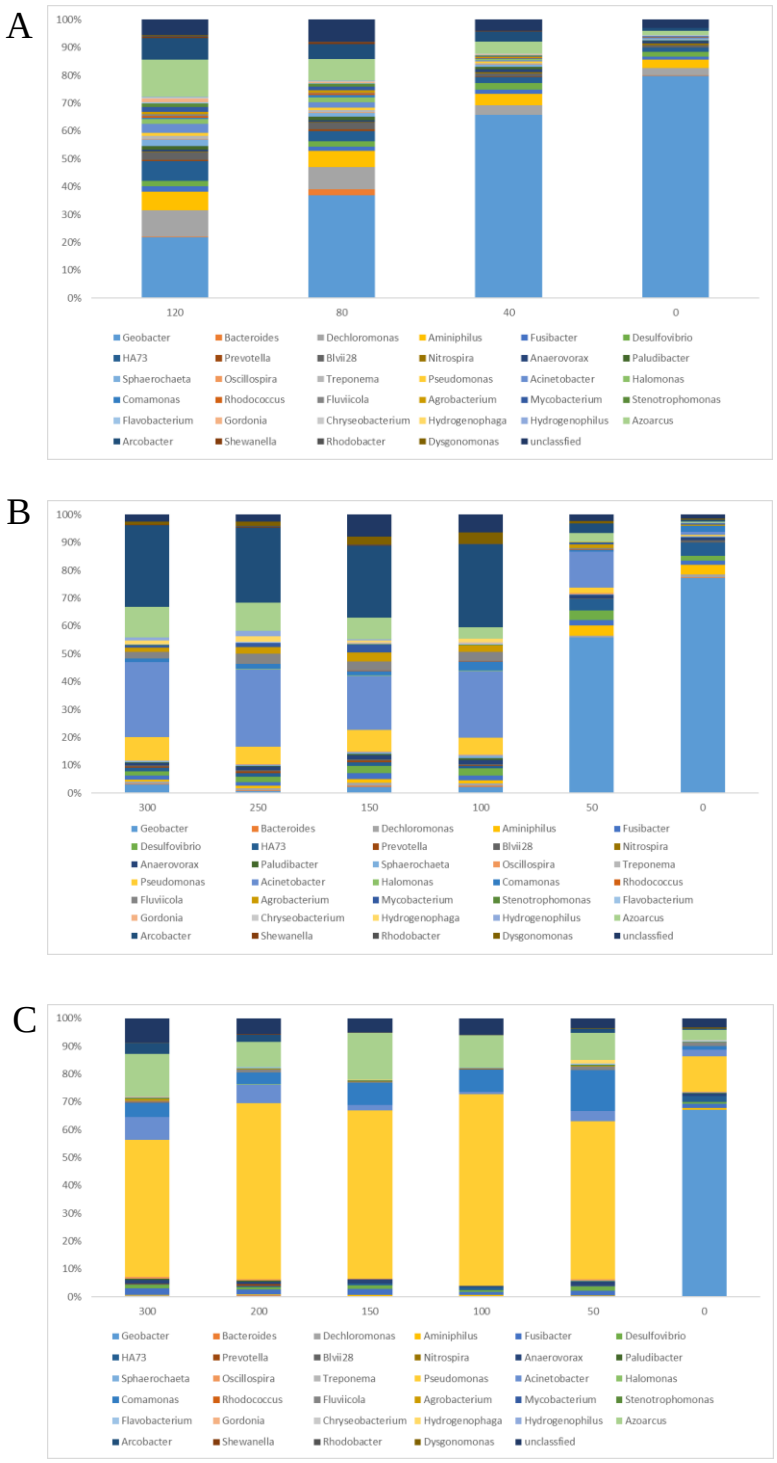

Figure S3. Bacterial communities based on MiSeq Illumina Sequencing for the anode biofilm enriched under OPP-0 (a), OPP-5 (b), OPP-15 (c). Related to Figure 3. The number of x axis represents the distance of sections from graphite surface.

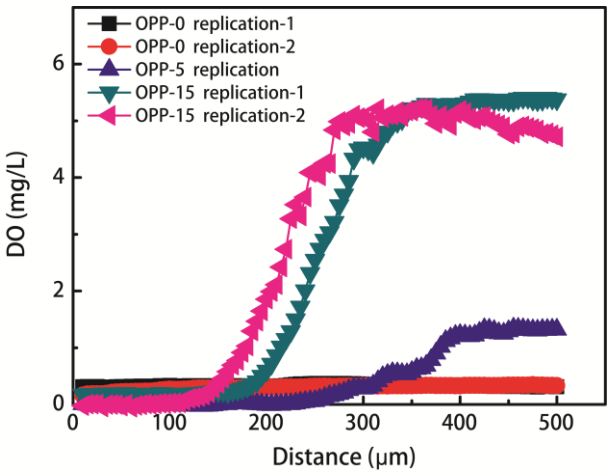

Figure S4. Oxygen distributions in the OPP-0, OPP-5 and OPP-15 anode biofilms.

Related to Figure 4. The distance 0 μm represent the graphite anode surface.

Transparent Methods

MFC configuration

Cubic dual-chamber air-cathode MFCs with a CEM (anode and cathode working volumes of 30 mL and 14 mL, respectively) were used in all the experiments (Figure S1). The anode and cathode were placed 6 cm apart at opposite ends of the MFC, and the CEM was placed at a distance of 2 cm from the cathode. The anodes were disk-shaped graphite plates (surface area of 3.14 cm^2, Shanghai Tansu Co., Ltd, China) that were polished with 400-grit and 800-grit abrasive papers and 0.05 μm alumina oxide powder and then were washed with 70% ethanol under ultrasonication followed by deionized water. The air cathodes (surface area of 7 cm^2) were composed of a nickel foam (Changle New Technology Electronics Co., Ltd, China) containing an activated carbon catalyst (Tianjin Yiborui Carbon Co. Ltd, China) (Cheng and Wu; 2013). Gas flow meters (Kede Instruments Co., Nanjing, China) were used to control the air and nitrogen flow rates to obtain gas mixtures with different oxygen partial pressures (total flow rate of 12 mL/min). The gas mixture was flowed over the anode surface from the bottom of the anode chamber and exited the chamber via a glass tube located at the top of the chamber.

MFC inoculation and operation.

During startup and operation, gas mixtures with oxygen partial pressures of 0%, 5%, 10%, 15% and 20% were continuously flowed through the MFCs, which were referred to as OPP-0, OPP-5, OPP-10, OPP-15 and OPP-20, respectively. The source of inoculum was a 5-L MFC reactor inoculated with the primary clarifier overflow of a

local wastewater treatment plant and fed with 50 mM PBS (2.45 g/L $NaH_2PO_4 \cdot H_2O$, 4.58 g/L Na_2HPO_4, 0.31 g/L NH_4Cl, 0.13 g/L KCl) containing 15 mM acetic acid (Yang and Cheng, 2019). The inoculum was the effluent of the 5-L MFC mixed with 1.5 g/L acetate, 12.5 mL/L trace minerals and 5 mL/L vitamins (Cheng et al., 2006). The oxygen concentration of the effluent was less than 0.5 mg/L. The anode chamber was immediately burbled after adding the inoculum. To maintain a constant dissolved oxygen (DO) concentration, the anode chamber was continuously aerated (except in the electrochemical analysis). During the setup and operation, the electrodes were continuously connected with a 1000 Ω external resistance (except in the electrochemical analysis). The cell and anode potentials were record using a digital data-collecting instrument (34970A, Agilent Technologies Co., USA). The anode and cathode solutions were replaced every 12 h, forming one cycle of operation. After all MFCs had reproducible cycles of voltage generation, the solution was switched to 50 mM PBS containing 1.5 g/L acetate, 12.5 mL/L trace minerals and 5 mL/L vitamins. The cathode solution was 50 mM PBS during both startup and operation. All tests were conducted in duplicates in a 30 °C temperature-controlled room (except as noted).

OCT observations

Anode biofilm growth was observed by spectral-domain OCT (SDOCT) in MB scanning mode (Li et al., 2016) every 24 h. The three-dimensional biofilm structure (z-stack) was reconstructed and analyzed using MATLAB software (MathWorks, USA), Jasc Animation Shop (Jasc, USA) and Amira (Visage Imaging, Australia). To ensure that each image captured the same area of the anode biofilm, the anode was placed in a

marked location without any sample preparation during the OCT observations.

Oxygen distribution in the anode biofilms

When all the MFCs had reached the stationary stage, the DO concentration in anode biofilms along the depth of the biofilm was measured by an oxygen microsensor connected to a multimeter (Unisense, Aarhus, Denmark) (Yuan et al., 2013; Wang et al., 2013). The microsensor was installed as shown in Figure S2. Before the measurements, the oxygen microsensor was polarized at -800 mV until the output signal was stable. During the measurements, the anode chamber was filled with 50 mM PBS containing 1.5 g/L acetate and always drummed the relevant mixture gas to keep the DO concentration constant in the solution. A stepper motor was used to control the microelectrode movement. The step length was set to 5 μm, and the DO concentration was recorded after every movement until the tip of the microsensor lightly touched the graphite surface and could not move forward.

Electrochemical analysis

The electrochemical analysis was performed after all the MFCs had reached the stationary stage for more than 20 cycles. LSV and EIS were performed in a three-electrode system using an electrochemical analyzer (Bio-Logic, Claix, France). The anode, the cathode and an Ag/AgCl electrode (0.201 mV vs SHE) were employed as the working, counter and reference electrodes, respectively. The Ag/AgCl reference electrode was placed in close proximity to the anode. The anode solution was refreshed before electrochemical analysis. LSV tests were performed three times in the potential range from -0.6 V to -0.1 V (vs Ag/AgCl) at a scan rate of 1 mV/s, and the data collected

in the third cycle were used for the analysis. EIS tests were conducted at the circuit voltage under an external resistance of 1000 Ω over the frequency range of 10^5-0.01 Hz with a 10-mV sinusoidal perturbation.

Frozen section

Samples for microbial community analyses were conducted when all the MFCs had reached the stationary stage for more than 30 cycles. Electrodes with mature anode biofilms were removed and rinsed twice with 50 mM PBS for 10 min. Then, the samples were immediately embedded in optimal cutting temperature compound (Sakura Tissue-Tek, USA) and flash frozen at -20 °C. The frozen sectioning of the anode was prepared on a cryostat (CryoStar™ NX70, Thermo Scientific, USA). During sectioning, the knife was kept parallel to the anode surface. The average section thickness was 10 μm. Each section was stored in a 2 mL centrifuge tube at -20 °C until further use.

Microbial community analysis

Section DNA was extracted using a DNA isolation kit (PowerSoil, USA). The community analysis was conducted via DNA extraction, PCR amplification (the paired primers in the V3-V4 variable regions used for PCR amplification were F: 5′-GTGCCAGCMGCCGCGGTAA-3′ and R: 5′-GGACTACHVGGGTWTCTAAT-3′), purification, database construction, and sequencing with the MiSeq Illumina sequencing platform as previously described (Sun et al., 2015). The returned sequences were clustered into operational taxonomic units (OTUs) using UPARSE software based on >97% similarity. A representative sequence of OTUs was analyzed using Silva128 Database based on VSEARCH algorithm to annotate taxonomic information.

Antibiotic tests

Antibiotic tests were performed after all MFCs had reproducible cycles of voltage generation (external resistance of 1000 Ω). Step 1: at the beginning of the cycle, the anode solution was refreshed with 50 mM PBS containing 1.5 g/L acetate, 12.5 mL/L trace minerals, 5 mL/L vitamins and antibiotics (metronidazole for OPP-5 and OPP-15, gentamicin for OPP-10 and OPP-20). Step 2: after 12 h of operation, all MFC anode solutions were refreshed (containing substrate) without the antibiotic and operated for 12 h. Step 3: step 1 was repeated. The concentrations of metronidazole and gentamicin were 120 mg/L and 48 mg/L, respectively, which were both at least two times higher than the minimum inhibitory concentration (MIC) to ensure the antibacterial effect (Song et al., 2013; Dione et al., 2015; Liu et al., 2017).

References

Cheng, S., Liu, H. and Logan, B.E. (2006). Increased power generation in a continuous flow MFC with advective flow through the porous anode and reduced electrode spacing. Environ. Sci. Technol. 40, 2426-2432.

Cheng, S. and Wu, J. (2013). Air-cathode preparation with activated carbon as catalyst, PTFE as binder and nickel foam as current collector for microbial fuel cells. Bioelectrochemistry 92, 22-26.

Dione, N., Khelaifia, S., Lagier, J. and Raoult, D. (2015). The aerobic activity of metronidazole against anaerobic bacteria. Int. J. Antimicrob. Ag. 45, 537-540.

Li, P., Cheng, Y., Zhou, L., Pan, C., Ding, Z. and Li, P. (2016). Single-shot angular

compounded optical coherence tomography angiography by splitting full-space B-scan modulation spectrum for flow contrast enhancement. Opt. Lett. 41, 1058

Liu, Z., Lin, Y., Lu, Q., Li, F., Yu, J., Wang, Z., He, Y. and Song, C. (2017). In vitro and in vivo activity of EDTA and antibacterial agents against the biofilm of mucoid *Pseudomonas aeruginosa*. Infection 45, 23-31.

Song, H., Guo, W., Liu, M. and Sun, J. (2013). Performance of microbial fuel cells on removal of metronidazole. Water Sci. Technol. 68, 2599-2604.

Sun, D., Cheng, S., Wang, A., Li, F., Logan, B.E. and Cen, K. (2015). Temporal-Spatial changes in viabilities and electrochemical properties of anode biofilms. Environ. Sci. Technol. 49, 5227-5235.

Wang, Z., Deng, H., Chen, L., Xiao, Y. and Zhao, F. (2013). In situ measurements of dissolved oxygen, pH and redox potential of biocathode microenvironments using microelectrodes. Bioresource Technol. 132, 387-390.

Yang, J., Cheng, S. (2019). Effects of using bacteria from anode biofilm and cathode biofilm as inoculum on the start-up, electricity generation and microbial community of air-cathode single-chamber microbial fuel cells. Pol. J. Environ. Stud. In press (Vol 29, No 2). Doi: 10.15244/pjoes/81700.

Yuan, Y., Zhou, S. and Tang, J. (2013). In situ investigation of cathode and local biofilm microenvironments reveals important roles of OH^- and oxygen transport in microbial fuel cells. Environ. Sci. Technol. 47, 4911-4917.